ISSN: 0067-2904

Comparing the Effect of In_2O_3 and Eu_2O_3 Impurities on the Structural and Optical Properties of Cerium Oxide

Mustafa M.Rasheed", Bushra A.Hasan
Department of physics, collage of science, university of Baghdad, Baghdad, Iraq

Received: 9/1/2023 Accepted: 20/3/2023 Published: 30/3/2024

Abstract

This work compares the changes in optical and structural properties of cerium oxide (CeO_2) when doped with different concentrations (3%,5%,7%, and 9%) of two oxides, In_2O_3 and Eu_2O_3. X-ray diffraction and spectrophotometry were employed in the visible, ultraviolet, and near-infrared regions. The findings demonstrated that CeO_2 doped with In_2O_3 and Eu_2O_3 thin films were polycrystalline and had a cubic structure. The crystal size increased from 20.5 to 32.15 when Eu_2O_3 doping ratio increased from 0% to 7% and then decreased to 28.46 nm at 9%. While the crystal size showed an increase from 20.5 to 21.42 nm with the increase of the In_2O_3 doping ratio, while the lattice constant measured for cubic CeO_2 changed opposite to that. The optical measurement showed that Eu_2O_3 and In_2O_3 doped CeO_2 thin films have a direct band gap with allowed transition with 3.0 eV for the undoped CeO_2. The band gap energy changed in a non-regular manner with the increase of the doping ratio of both oxides. The minimum band gap energy was 1.2 eV obtained for 7% Eu_2O_3 doped CeO_2 thin film, and the minimum band gap energy was 1.4 eV obtained for 9% In_2O_3 doped CeO_2. These results qualify them for use as absorbers in solar cell applications.

Keywords: cerium oxide, indium oxide, europium oxide, x-ray diffraction, optical properties.

مقارنة تأثير شوائب In_2O_3 و Eu_2O_3 على الخصائص التركيبية والبصرية لأكسيد السيريوم

مصطفى مثنى رشيد*, بشرى عباس حسن
قسم الفيزياء, كلية العلوم, جامعة بغداد, بغداد, العراق

الخلاصة

هذا العمل يقارن التغييرات في الخواص التركيبية والبصرية لاوكسيد السيريوم بتشويبه باوكسيدين مختلفين هما اوكسيد اليوريبوم واوكسيد الانديوم . فقد تم فحص الخواص التركيبية والبصرية للمادة الاولية وهي اوكسيد السيريوم عند تشويبها بنسب مختلفة (3%,5%,7%, and 9%) من الاوكسيدين. ولهذا الغرض تم توظيف حيود الاشعة السينية والمطياف البصري عند المنطقة فوق البفسجية والمرئية وتحت الحمراء. اظهرت النتائج ان اغشية اوكسيد السيريوم غير المشوبة والمشوبة باوكسيد اليوريبيوم والانديوم كانت متعددة البلورات وبتركيب مكعب الشكل. لقد وجدت ان حجم البلورة قد ازدادت من 20.5 الى 32.15 نانوميترعند زيادة نسبة اوكسيد اليوريبوم من 0% الى 7% ثم تقل الى 28.46 نانوميترمع زيادة نسبة اوكسيد اليوريبوم لكن حجم البلورة أظهرت زيادة مضطردة من 20.5 الى 21.42 نانوميتر مع زيادة نسبة التشويب باوكسيد الانديوم بينما أظهرت النتائج بأن ثابت الشبيكة للتركيب المكعبي لاوكسيد السيريوم ذو تغير معاكس لذلك. بينت القياسات

*Email: mustafamuthana79@gmail.com

البصرية ان اوكسيد السيريوم غير المشوب له فجوة طاقة مقدارها 3.0 الكترون فولت للانتقال المباشر والمسموح .اظهرت فجوة الطاقة البصرية تغيرا غير منتظما مع زيادة نسبة التشويب لكلا الاوكسيدين .ان اقل فجوة طاقة بصرية تم الحصول عليها كانت 1.2 الكترون فولت للغشاء الرقيق عند نسبة التشويب 7% باوكسيد اليوريبيوم وهذا يجعله صالحا للاستخدام كطبقة ماصة في تطبيقات الخلايا الشمسية.

1. Introduction

In the past 20 years, significant advancements have been made in creating new mesostructured and mesoporous materials with different pore structures and dimensions [1]. Cerium oxide (CeO_2) based materials have drawn a lot of attention because of their widespread use in numerous application fields, including the production of hydrogen, gas sensing, catalysis, and electrodes in fuel cells [2]. In the area of micro-electronics, CeO_2 is viewed as a high κ-gate oxide material as a result of its unique characteristics: moderate band gap (3eV–3.6eV), high refractive index (n: 2.20–2.80), high dielectric constant (κ: 23–26), and high dielectric strength (approximately 2.6MV/cm) [3]. CeO_2 is also suitable for silicon-based Metal Oxide Semiconductor (MOS) devices because of its small lattice mismatch (about 0.35%) with silicon favoring its epitaxial growth on various silicon surfaces and low density of the interface state (about $10^{11}cm^{-2}eV^{-1}$) [4].

Europium oxide (Eu_2O_3), a rare earth oxide, is particularly appealing due to its wide band gap of 3.7eV [5], high dielectric constant, and exceptional properties of significant conduction band displacement. Eu_2O_3 has lately been researched and utilized in numerous new technologies, including microelectronic, optical, and telecommunications devices. Eu_2O_3 differs from ordinary semiconductors in that it has a novel model of the energy zone that includes the valence band, conduction band, and the very narrow 4f group [5].

Indium oxide (In_2O_3) is a widely studied oxide frequently generated as a single crystal or thin film. Energy-efficient windows, solar cells, Schottky contacts, thin film transistors, and diodes are some optoelectronic and electronic applications for In_2O_3 [6]. In_2O_3 is also used in a wide range of ceramic applications. The availability of bulk samples and thin films with good crystalline quality has increased the interest in integrating In_2O_3 into device applications over the past few decades [6].

The present work aimed to explore the effect of doping with In_2O_3 and Eu_2O_3 on the structural and optical properties of the starting materials CeO_2 to determine the suitable application for erbium and indium doped ceria. The current research involved preparing In_2O_3 and Eu_2O_3 doped CeO_2 films on glass substrates using the Pules Laser Deposition (PLD) technique. The structural and optical analysis of In_2O_3 and Eu_2O_3 doped CeO_2 films were examined.

2-Experimental

In this work, CeO_2, Eu_2O_3 and In_2O_3 oxides with high purity (99.999) were used. Different compounds with various doping ratios based on atomic weight were weighted with an electronic balance with four digits after the point (10^{-4}gm). The required amount of CeO_2 doped with Eu_2O_3 and In_2O_3 compounds were put in a quartz ampoule of a length of approximately 25cm and internal diameter of ~ 8mm, which was evacuated to about 10^{-3} Torr and heated in an oven at 1273 K and left at this temperature for one hour then left to cool to room temperature at 303K. The obtained compounds from (CeO_2:Eu_2O_3 and In_2O_3) were ground and pressed into pellets shapes under a pressure of 7 tons for 15 secs. The pellets were 1 cm in diameter and 0.5 cm in thickness. Nine types of targets from (CeO_2: Eu_2O_3 and In_2O_3) with a variety of doping

ratios (0, 0.03, 0.05, 0.07, & 0.09) were used to prepare thin films using the PLD method. The deposition was performed in a vacuum of 2 x 10^{-2} Torr using Nd:YAG laser beam (with energy of 500mJ, pulse of 200 shoots, and frequency of 6 Hz), which was focused through a window to be incident on the target. The ablated atoms from the target deposited and gathered on the glass substrates creating thin films.

The film thickness (t) was determined using Fizaeu fringes given by:

$$t = \frac{\lambda}{2}\frac{\Delta x}{x} \quad (1)$$

Where: Δx, x and λ represent shifting between interference fringes, the distance between the interference fringes and the wavelength of He: Ne (589.3 nm), respectively. Crystal structure and crystallinity of Eu_2O_3 doped CeO_2 and In_2O_3 doped CeO_2 thin films were determined by the XRD technique with the CuKα radiation (λ= 1.5406Å). The optical measurements were made using a UV-Visible spectrophotometer of wavelength range (190-1100) nm; both the absorbance and the transmittance of the (CeO_2): (Eu_2O_3, In_2O_3) thin films were determined.

$$\alpha=2.303A/t \quad (2)$$

Equation (2) was used to calculate the absorption coefficient, where A represents absorbance and t is the thin film thickness. The optical energy gap was estimated by the Tauc relation for direct permitted transitions [7]:

$$(\alpha h\nu) = B(h\nu - E_g)^r \quad (3)$$

Where: B represents a constant, and E_g represents the optical band gap energy. The equations utilized to measure the optical constants, including refractive index, extinction coefficient, and real and imaginary dielectric constants, are:

$$n = (4R/(R-1)^2 - k^2)^{1/2} - (R+1)/(R-1) \quad (4)$$

$$R = (n-1)^2 + k^2/ (n+1)^2 + k^2 \quad (5)$$

$$\varepsilon_r = n^2-k^2 \quad (6)$$

$$\varepsilon_i = 2nk \quad (7)$$

where the reflectance (R)is calculated from the relation:

$$R= 1-(A+T) \quad (8)$$

3- Result and discussion

3-1 Structural properties

3-1-1 Structural analysis of (CeO_2):(Eu_2O_3) thin films

XRD analysis was utilized to determine the phase purity crystal structure of Eu_2O_3 doped CeO_2. Figure 1 shows the XRD patterns for the pure CeO_2 and Eu_2O_3doped CeO_2 thin films.

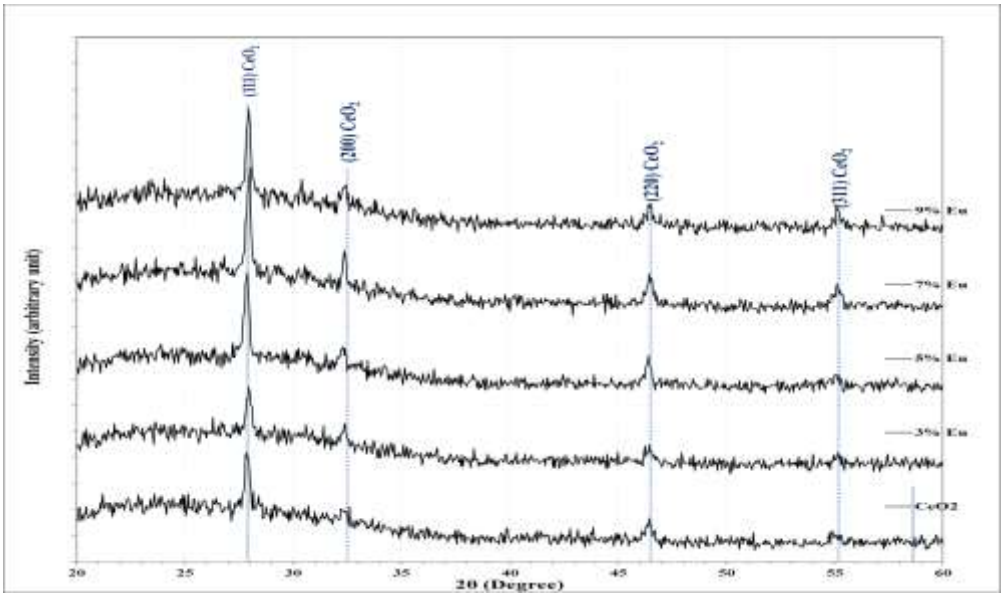

Figure 1: XRD patterns for the pure CeO_2 and Eu_2O_3doped CeO_2 thin films

CeO_2 is responsible for the principal reflections that may be detected in the diffraction patterns. The (111), (200), (220), and (311) planes are all reflection peaks that are well indexed and detected to pure CeO_2, which has the cubic fluorite phase (these data coincided with JCPDS (The Joint Committee on Powder Diffraction Standards) data) [8]. Table 1 gives the obtained values from the XRD patterns for (CeO_2):(Eu_2O_3)thin films. These data are consistent with the findings of Sharma et al. [9].

Table 1: XRD obtained data of (CeO_2):(Eu_2O_3)thin films

Eu%	2θ (Deg.)	FWHM (Deg.)	d_{hkl} (Å)	C.S (nm)	hkl	Phase	Card No.	ε
0	27.8721	0.3059	3.1984	26.8	(111)	Cub. CeO_2	96-434-3162	0.0013
	32.3391	0.4589	2.7661	18.0	(200)	Cub. CeO_2	96-434-3162	0.0019
	46.4627	0.4079	1.9529	21.2	(220)	Cub. CeO_2	96-434-3162	0.0016
	55.0287	0.5609	1.6674	16.0	(311)	Cub. CeO_2	96-434-3162	0.0031
3	27.9041	0.3315	3.1948	24.7	(111)	Cub. CeO_2	96-434-3162	0.0014
	32.3901	0.3059	2.7618	27.1	(200)	Cub. CeO_2	96-434-3162	0.0013
	46.5137	0.4334	1.9508	20.0	(220)	Cub. CeO_2	96-434-3162	0.0017
	55.1562	0.5354	1.6639	16.7	(311)	Cub. CeO_2	96-434-3162	0.0031
5	27.9276	0.3059	3.1922	26.8	(111)	Cub. CeO_2	96-434-3162	0.0013
	32.2626	0.3569	2.7725	23.2	(200)	Cub. CeO_2	96-434-3162	0.0015
	46.4117	0.2804	1.9549	30.8	(220)	Cub. CeO_2	96-434-3162	0.0011
	55.1307	0.4589	1.6646	19.5	(311)	Cub. CeO_2	96-434-3162	0.0031
7	27.9600	0.2550	3.1885	32.1	(111)	Cub. CeO_2	96-434-3162	0.0011
	32.3646	0.2039	2.7640	40.6	(200)	Cub. CeO_2	96-434-3162	0.0009
	46.4882	0.2550	1.9519	33.9	(220)	Cub. CeO_2	96-434-3162	0.0010
	55.1816	0.4079	1.6632	22.0	(311)	Cub. CeO_2	96-434-3162	0.0031
9	27.9541	0.2410	3.1892	34.0	(111)	Cub. CeO_2	96-434-3162	0.0010
	32.4920	0.3100	2.7534	26.7	(200)	Cub. CeO_2	96-434-3162	0.0013
	46.4627	0.3314	1.9529	26.1	(220)	Cub. CeO_2	96-434-3162	0.0013
	55.1562	0.3314	1.6639	27.1	(311)	Cub. CeO_2	96-434-3162	0.0031

The value of d spacing belonging to the (111) plane decreased with the increase of the Eu_2O_3 doping ratio, reflecting a reduction in lattice characteristics. This effect is anticipated given the difference between ionic radii of Ce and Eu; Eu^{+3} ions' ionic radius is 0.1066 nm less than Ce^{+4} ions' of 0.0970 nm. X-ray diffraction pattern showed that Eu had replaced Ce ions in CeO_2. The [111] plane of CeO_2's FWHM (The Full Width at Half Maximum) values indicated an increase in crystallinity that coincided with the introduction of Eu^{+3} ions to the oxide lattice, as can be seen in Table 2.

Table 2 displays the computed lattice parameters for the Eu-doped and pristine ceria samples.

It is demonstrated that growing crystallite size results in the removal of defects like oxygen vacancies as well as a decrease in strain values [10-14]

Table 2: The lattice constant and average crystal size for pure CeO_2 and Eu_2O_3doped CeO_2 thin films

x	a (Å)	Average C.S (nm)
0	5.5398	18.82
3	5.5336	22.12
5	5.5290	25.08
7	5.5227	32.15
9	5.5239	28.46

The XRD pattern is free from any impurity peaks indicating good incorporation of Eu into the lattice sites of CeO_2, or the amount is too small to be detected by XRD.

3-1-2 Structural analysis of CeO_2: In_2O_3 thin films

The XRD patterns of pure CeO_2 and In_2O_3 doped CeO_2 thin films are depicted in Figure 2.

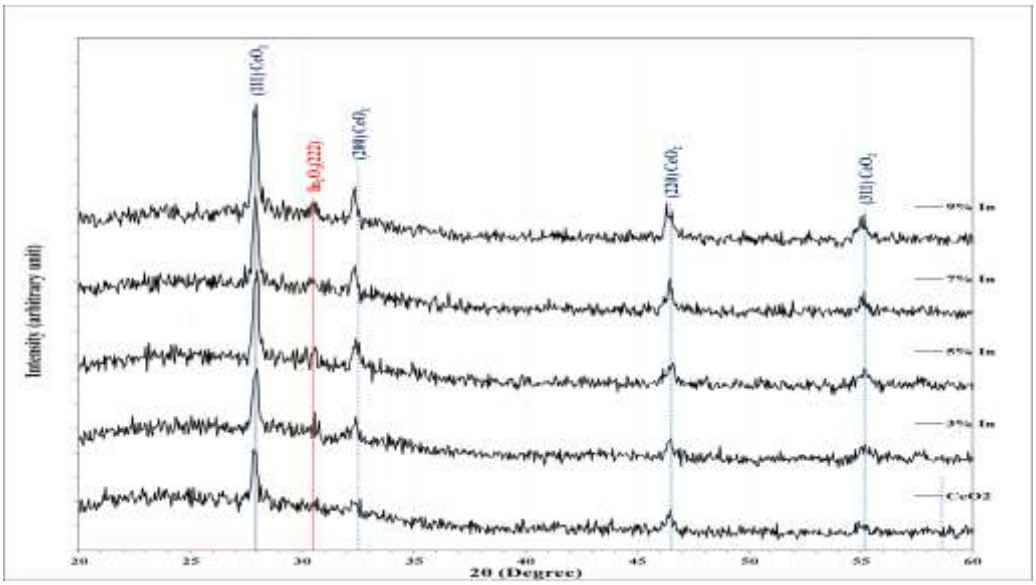

Figure 2: XRD patterns of pure CeO_2 and In_2O_3 doped CeO_2 thin films

XRD pattern of the pure CeO_2 showed distinctive peaks at 2θ of 27.8636º, 32.2442º, 46.4632º and 55.1167º, corresponding to (111), (200), (220) and (311) planes of CeO_2 (as shown in Table 3).

Table 3: The XRD obtained data of CeO_2:In_2O_3 thin films.

In%	2θ (Deg.)	FWHM (Deg.)	d_{hkl} (Å)	C.S (nm)	hkl	Phases	Card No.	ε
0	27.8636	0.3232	3.1994	25.3	(111)	Cub. CeO_2	96-434-3162	0.0014
	32.2442	0.3591	2.7740	23.0	(200)	Cub. CeO_2	96-434-3162	0.0015
	46.4632	0.5386	1.9529	16.1	(220)	Cub. CeO_2	96-434-3162	0.0022
	55.1167	0.8259	1.6650	10.9	(311)	Cub. CeO_2	96-434-3162	0.0031
3	27.9713	0.3591	3.1873	22.8	(111)	Cub. CeO_2	96-434-3162	0.0015
	32.3878	0.4309	2.7620	19.2	(200)	Cub. CeO_2	96-434-3162	0.0018
	46.4632	0.5026	1.9529	17.2	(220)	Cub. CeO_2	96-434-3162	0.0020
	55.1167	0.6822	1.6650	13.1	(311)	Cub. CeO_2	96-434-3162	0.0031
5	28.0072	0.3232	3.1833	25.3	(111)	Cub. CeO_2	96-434-3162	0.0014
	32.3878	0.3949	2.7620	21.0	(200)	Cub. CeO_2	96-434-3162	0.0017
	46.4632	0.4309	1.9529	20.1	(220)	Cub. CeO_2	96-434-3162	0.0017
	55.1167	0.8259	1.6650	10.9	(311)	Cub. CeO_2	96-434-3162	0.0031
7	27.8995	0.3232	3.1953	25.3	(111)	Cub. CeO_2	96-434-3162	0.0014
	30.4847	0.5386	2.9300	15.3	(222)	Cub. In_2O_3	96-101-0589	0.0023
	32.3519	0.3591	2.7650	23.0	(200)	Cub. CeO_2	96-434-3162	0.0015
	46.4273	0.3949	1.9543	21.9	(220)	Cub. CeO_2	96-434-3162	0.0016
	55.1167	0.5027	1.6650	17.8	(311)	Cub. CeO_2	96-434-3162	0.0031
9	27.9354	0.3232	3.1913	25.3	(111)	Cub. CeO_2	96-434-3162	0.0014
	30.5206	0.5027	2.9266	16.4	(222)	Cub. In_2O_3	96-101-0589	0.0021
	32.3519	0.3231	2.7650	25.6	(200)	Cub. CeO_2	96-434-3162	0.0014
	46.2837	0.3949	1.9600	21.9	(220)	Cub. CeO_2	96-434-3162	0.0016
	54.9731	0.5027	1.6690	17.8	(311)	Cub. CeO_2	96-434-3162	0.0031

The synthesized thin films crystalline structure was cubic rutile based on JCPDS reference data [8]. Additional peaks can be seen located at 2θ of 30.48 and 30.52 º at doping ratios of 7% and 9% corresponding to the plane (222) related to cubic indium oxide. It was noted that there was a secondary phase at the high doping ratio corresponding to cubic indium oxide. The value of 2θ of the main plane (111) was shifted to higher angles compared with the pure CeO_2. This occurs due to lattice parameters contraction, as shown in Table 4, indicating a reduction in the crystal lattice parameter (a). This is a result of the substitution of smaller In ion [ionic radius (In^{+3} =0.79 nm] for Ce [ionic radius (Ce^{+4}) =0.97 nm] [15,16]. The reduction of strain, as shown in the same table, causes the growth of crystallite size.

Table 4: The lattice constant and average crystal size for pure CeO_2 and In_2O_3doped CeO_2 thin films

x	a (Å)	Average C.S (nm)
0	5.5415	18.82
3	5.5205	18.09
5	5.5136	19.31
7	5.5345	20.68
9	5.5275	21.41

3-2 Optical properties

3-2-1 Optical characteristics of Eu_2O_3 doped CeO_2 thin films

The optical transmission data (the absorption spectra) was obtained with a UV-Vis spectrophotometer. The transmittance spectra of Eu_2O_3 doped CeO_2 thin films, depicted in Figure 3, were evaluated to investigate the optical characteristics, as depicted in Figure 3.

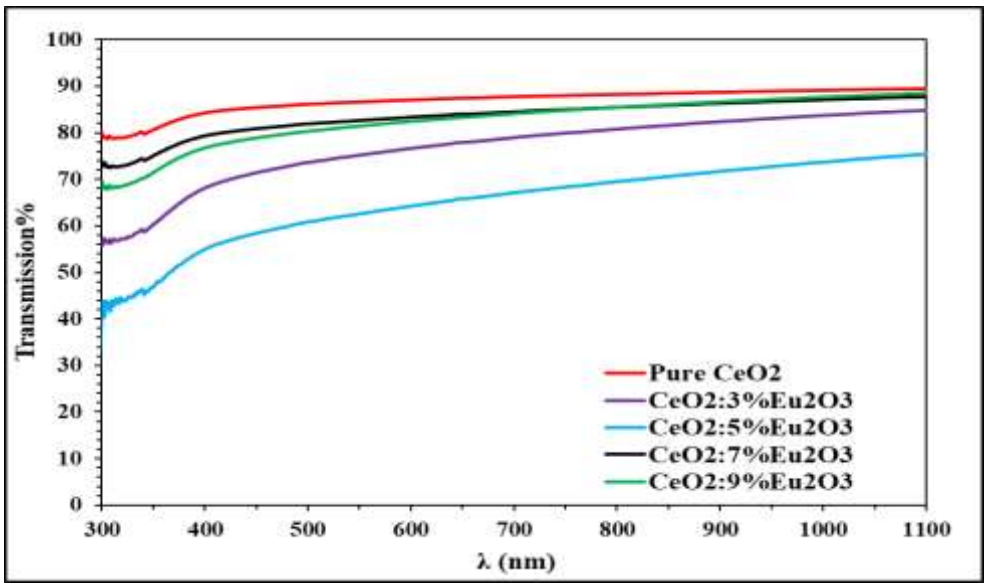

Figure 3: Transmittance spectra of the pure CeO_2 and Eu_2O_3 doped CeO_2 thin films.

CeO_2 thin film has high transparency and average transmittance higher than 89% in the visible range. When Eu_2O_3 concentration was increased in the starting material, one can notice, besides variation of the film color (from transparent to brown), a variation in the average transmittance, approximately 55-75% for Eu_2O_3 doped CeO_2 films.

As can be seen from Figure 4, the value of the direct band gap energy of pure CeO_2 thin film is 3 eV. The values were 2.9, 2.82, 1.2 and 1.25eV for Eu_2O_3 doped CeO_2 thin films with doping ratios of (0.03, 0.05, 0.07 and 0.09), respectively. The maximal value of 3 eV was obtained for undoped CeO_2. The energy band gap values of CeO_2 agree with that reported by Bouhlala et al. [17] and Kumar et al. [18]

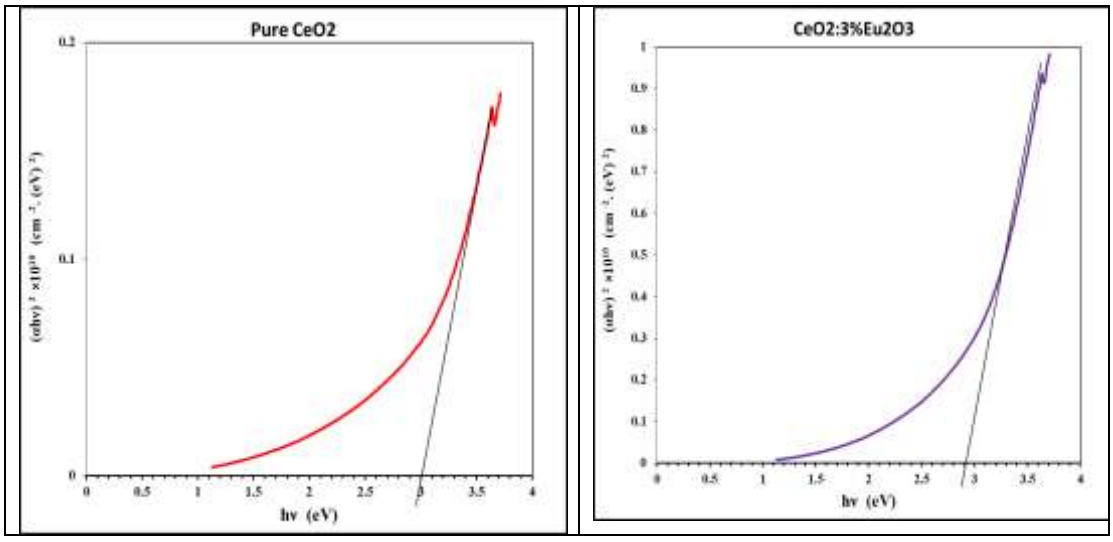

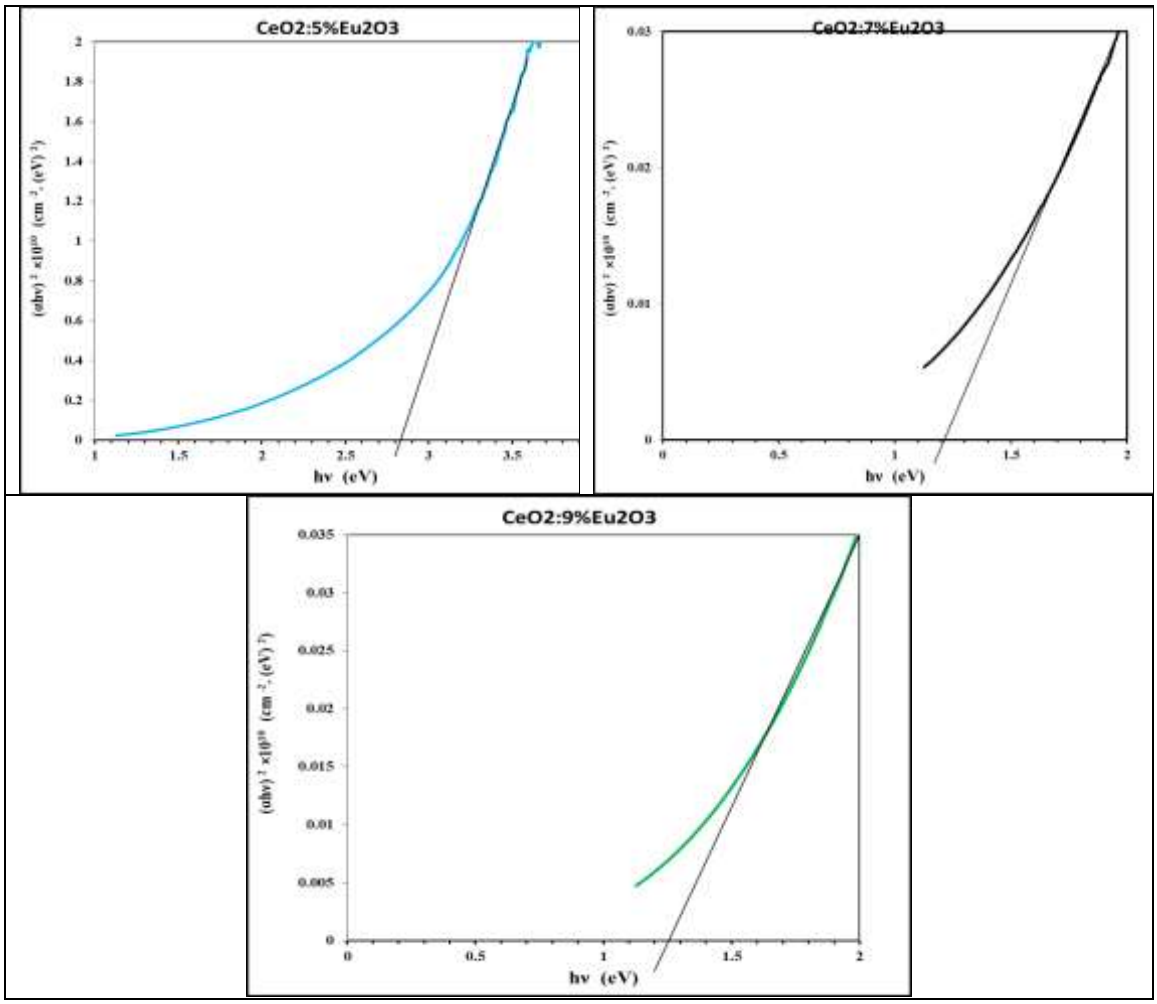

Figure 4: Determination of the optical energy gap of(CeO_2:Eu_2O_3)

Figures 5 to 8 show plot diagrams of the refractive index, extinction coefficient, refractive index, and real and imaginary parts of the dielectric constant for pure CeO_2 and Eu_2O_3 doped CeO_2 thin films. It is clear that the addition of Eu_2O_3 oxide to CeO_2 oxide has changed the optical constant but in different manners depending on the added amount.

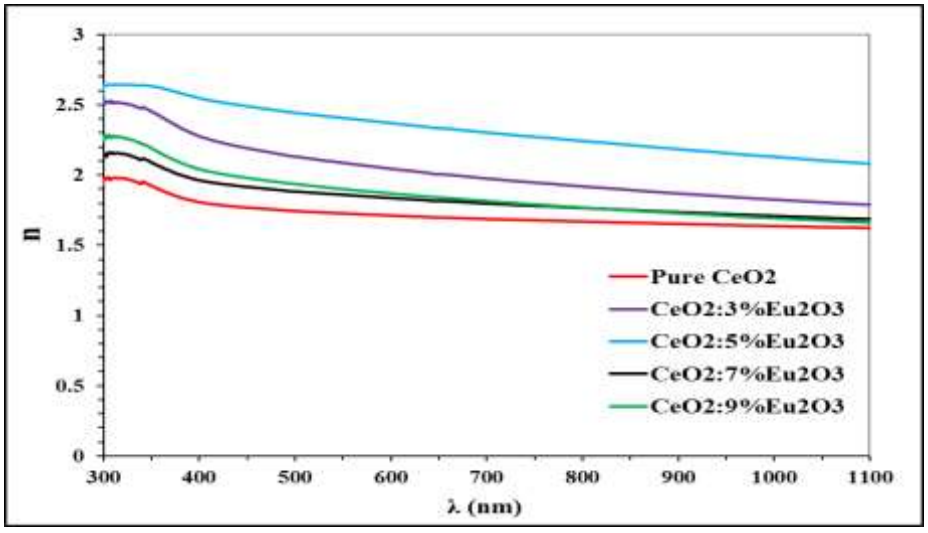

Figure 5: Refractive index as a function of wavelength for pure CeO_2 and Eu_2O_3 doped CeO_2 thin films.

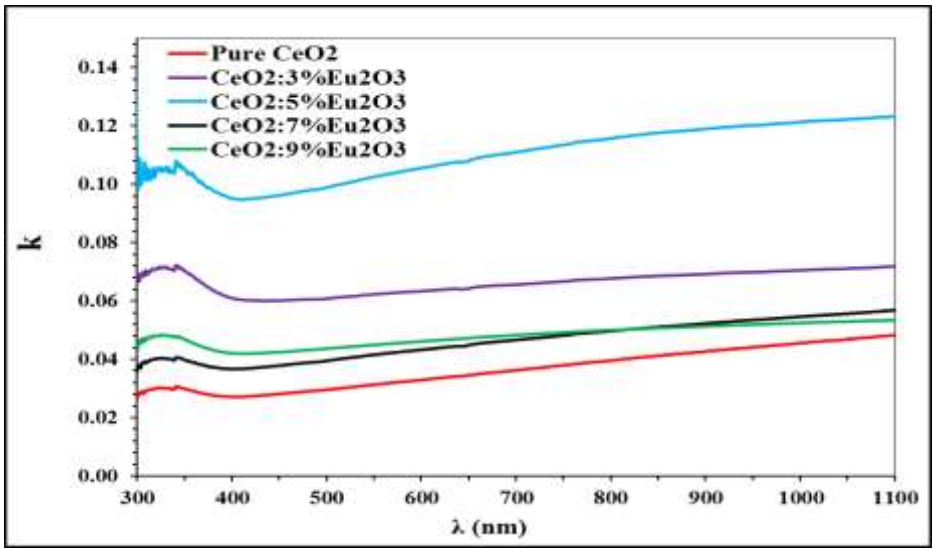

Figure 6: Extinction coefficient as function of wavelength for pure CeO_2 and Eu_2O_3 doped CeO_2 thin films.

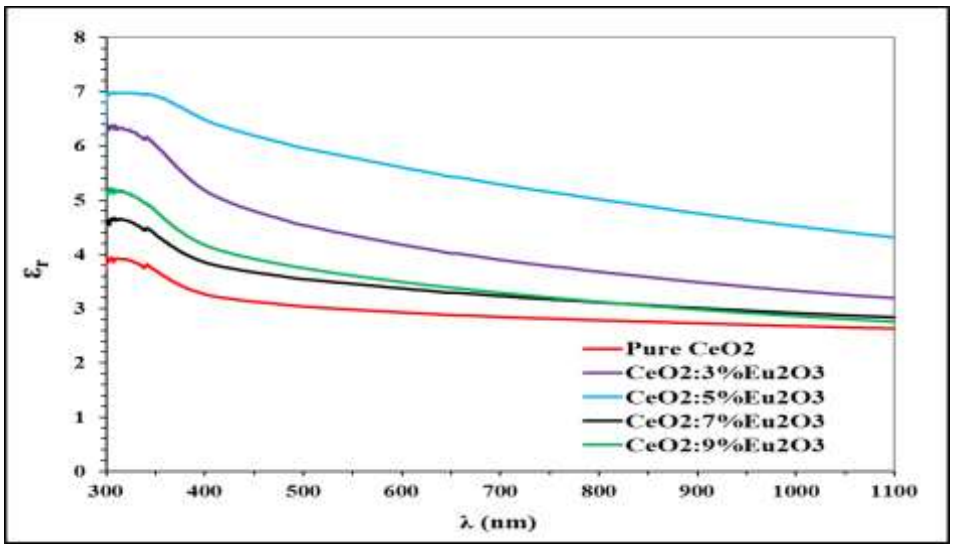

Figure 7: Real dielectric constant as a function of the wavelength for the pure CeO_2 and Eu_2O_3 doped CeO_2 thin films.

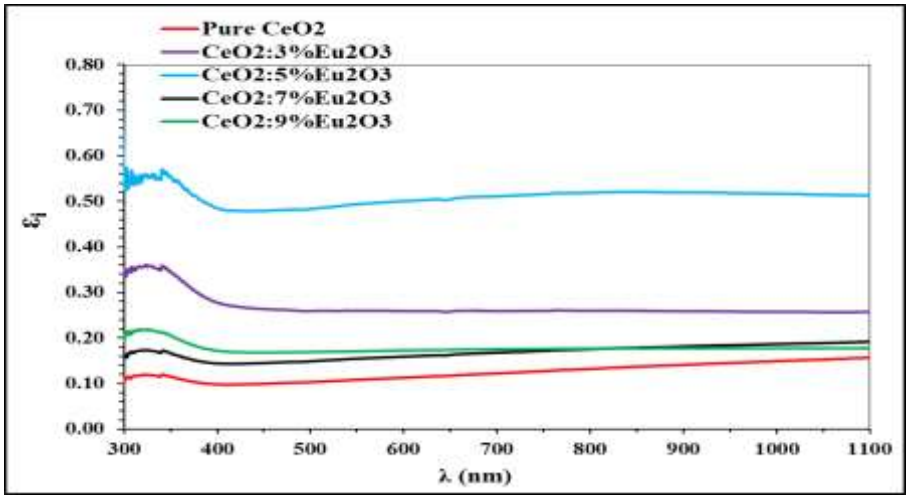

Figure 8: Imaginary dielectric constant as function of the wavelength for the pure CeO_2 and Eu_2O_3 doped CeO_2 thin film

In general, the addition of Eu_2O_3 oxide reduced transmittance and hence all the optical constant values (n, k, ε_r, and ε_i). They increased with the increase of the doping ratios (3%-5%), they decreased at (7%), and then increased at (9%), as shown in Table 5.

Table 5: transmittance, absorption coefficient, optical properties at λ=550 nm and optical energy gap of CeO_2: Eu_2O_3 thin film that have been prepared using the PLD technique

Samples	T%	α (cm^{-1})	k	n	ε_r	ε_i	Eg (eV)
Pure CeO2	86.70	7139	0.031	1.727	2.981	0.108	3.00
CeO2:3%Eu2O3	75.25	14221	0.062	2.087	4.352	0.260	2.90
CeO2:5%Eu2O3	62.63	23404	0.102	2.407	5.781	0.493	2.82
CeO2:7%Eu2O3	82.70	9500	0.042	1.861	3.460	0.155	1.20
CeO2:9%Eu2O3	81.47	10248	0.045	1.900	3.608	0.171	1.25

3-2-2 Optical characteristics of In_2O_3 doped CeO_2 thin films

In the wavelength range of 300nm-1100nm, the optical transmittance spectra of the pure and In_2O_3 doped CeO_2 thin films were studied. The spectra, depicted in Figure 9, demonstrated that the produced thin films had a mean transmittance that varies between 70 and 80% in the visible range. For pure CeO_2 film, a high level of transparency was noted. Nevertheless, the films transmittances reduced as the doping levels were increased. It is common knowledge that excessive surface roughness increases light diffusion, which lowers transmittance. The cut-off wavelength for all of the films was roughly 300 nm in the ultraviolet region.

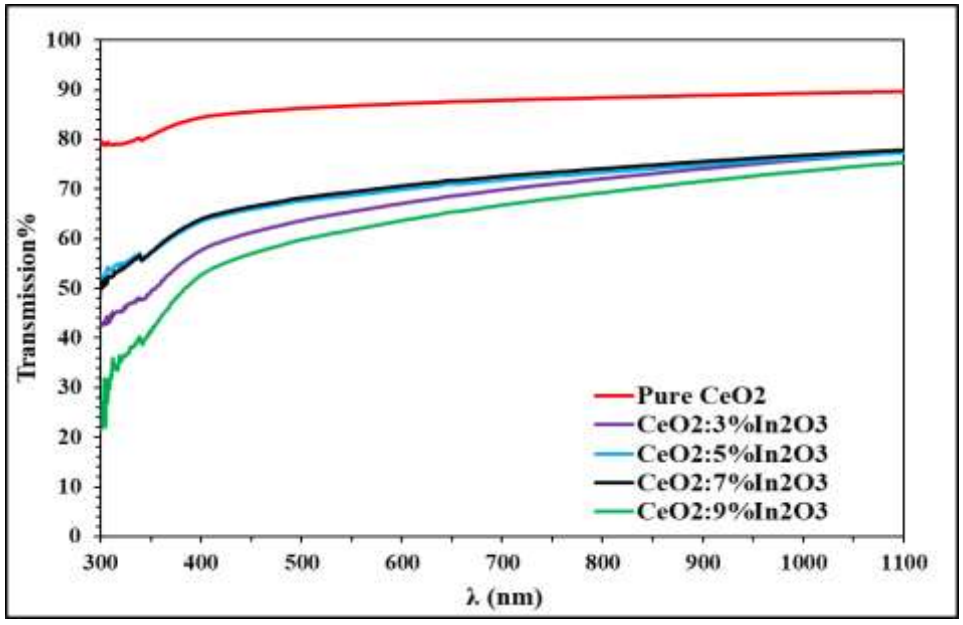

Figure 9: Transmission spectra for pure CeO_2 and In_2O_3 doped CeO_2

The energy values of the direct band gap were 3.00, 2.9, 2.85,2.90 and 1.55 eV for the pure and In_2O_3 doped CeO_2 of the different doping ratios thin films, as seen in Figure 10. The maximum value of 3.00 was obtained for pure CeO_2. It is obvious that the band gap energy showed regular reduction by increasing the doping ratio. As a result of the absorption coefficient increase, only the 9% In_2O_3 doped ceria thin film revealed indirect permitted transition where r = 0.5 and the energy gap was estimated to be 1.4 eV, as shown in Figure 10 and Table 6.

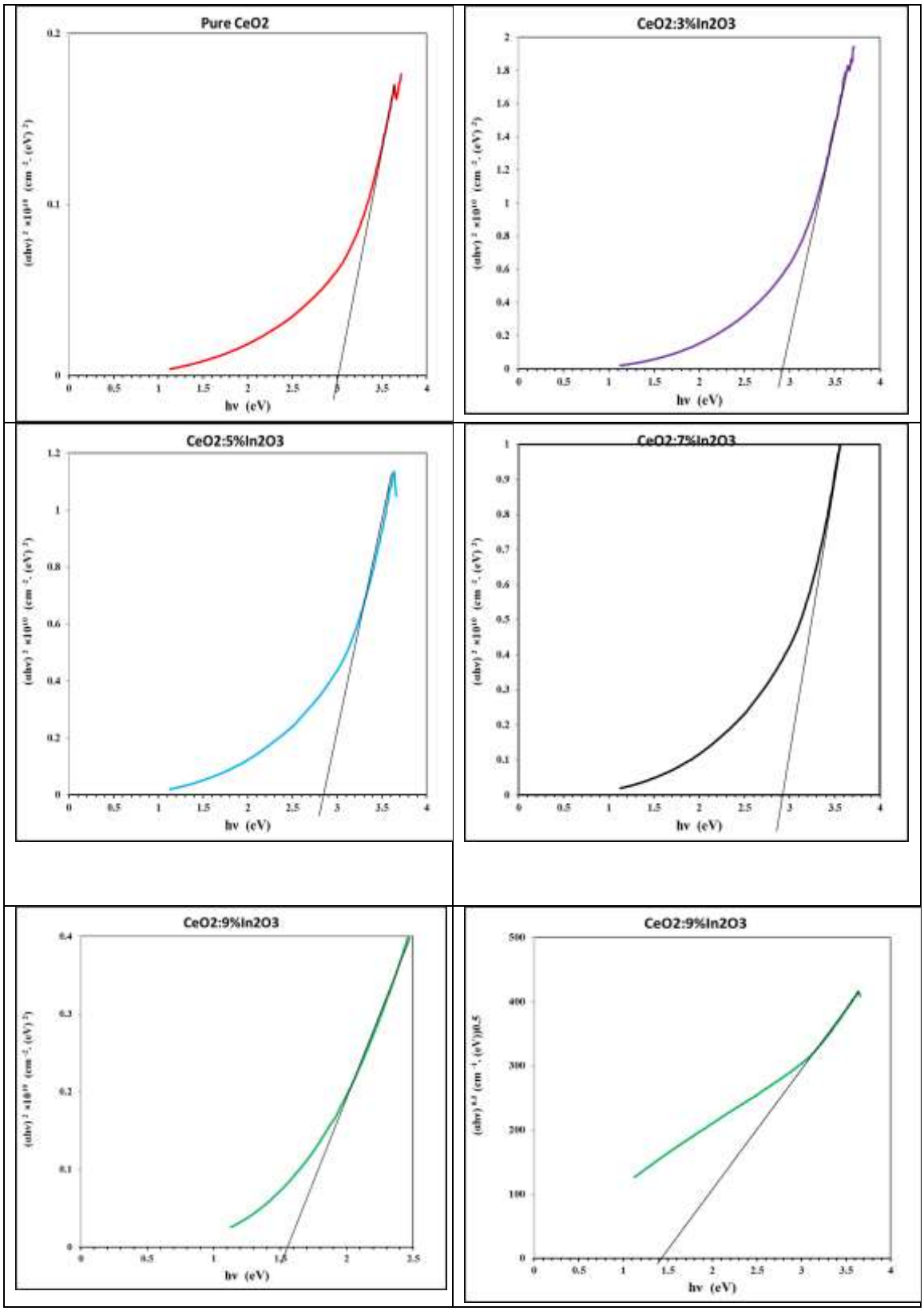

Figure 10: Determination of the optical energy gap of(CeO_2:In_2O_3**)**

Figure 11 to 14 show plot diagrams of extinction coefficient, refractive index, and real and imaginary parts of dielectric constant for the pure CeO_2 and In_2O_3 doped CeO_2 thin films.

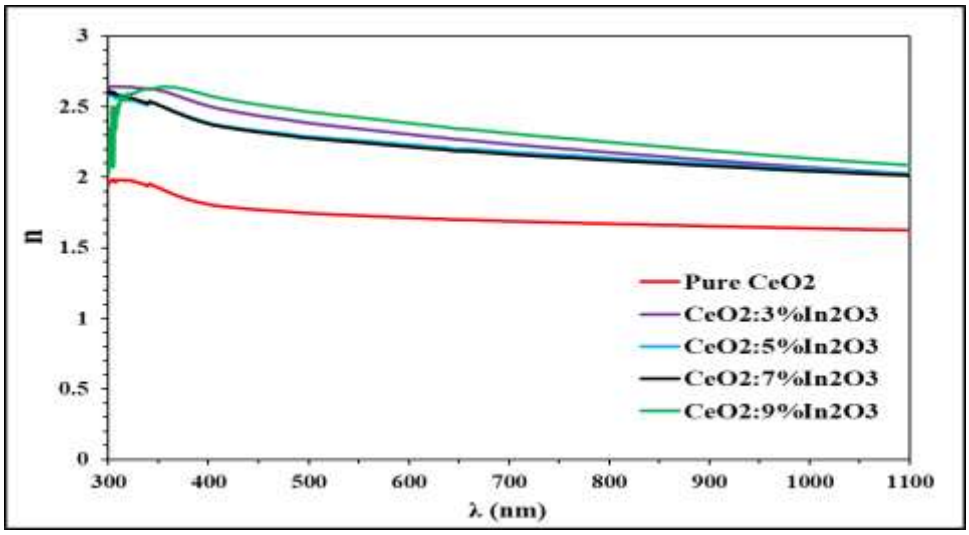

Figure 11: Refractive index as function of the wavelength for the pure CeO_2 and In_2O_3 doped CeO_2 thin films.

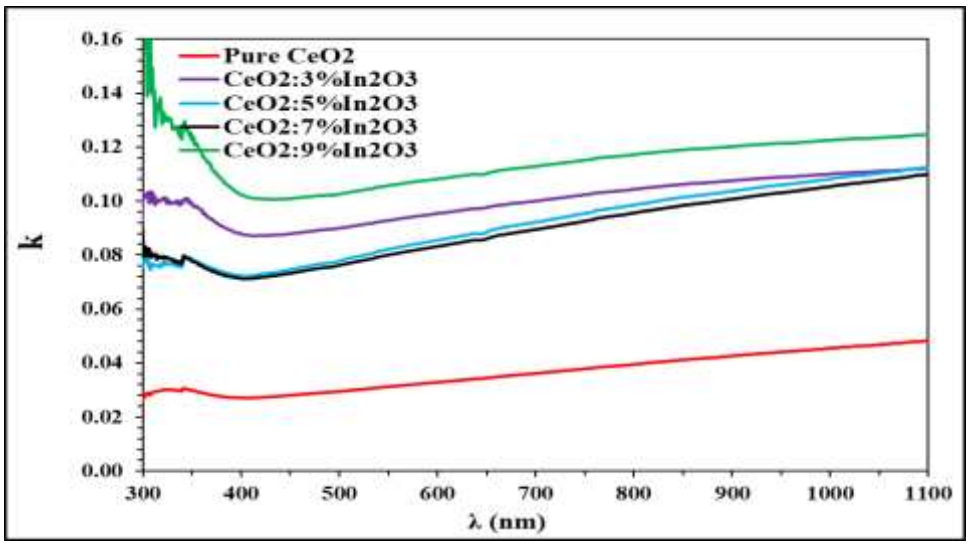

Figure 12: Extinction coefficient as function of the wavelength for pure CeO_2 and In_2O_3 doped CeO_2 thin films.

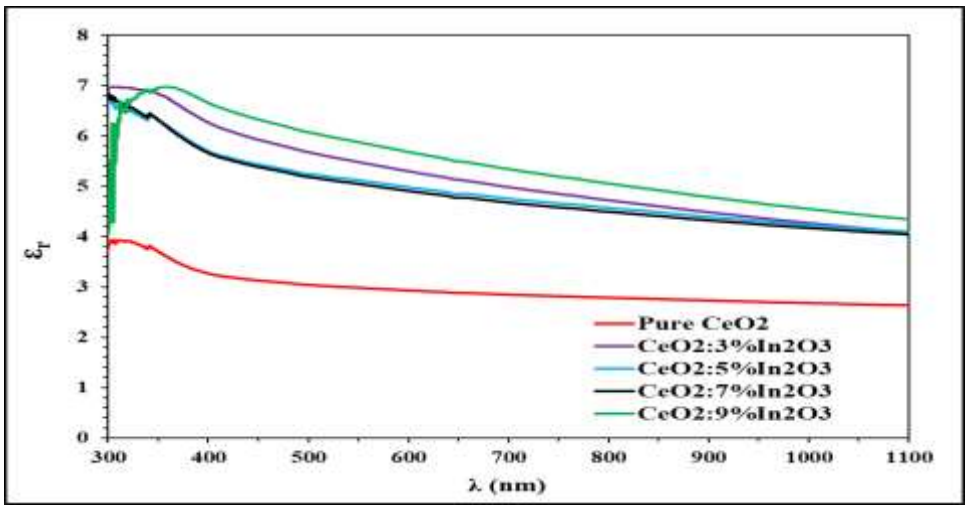

Figure 13: Real dielectric constant as function of the wavelength FOR pure CeO_2 and In_2O_3 doped CeO_2 thin films.

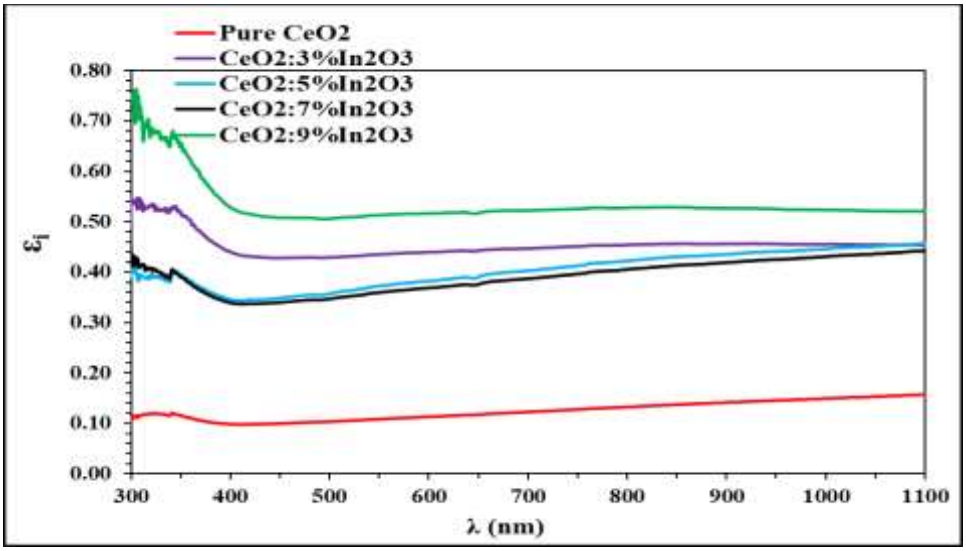

Figure 14: Imaginary dielectric constant as function of the wavelength for pure CeO_2 and In_2O_3 doped CeO_2 thin film

It is clear that the addition of In_2O_3 oxide to CeO_2 oxide increased the transmittance and hence reduced the values of the optical constants (n, k, ε_r, and ε_i). All have the highest value at 9% doping concentration, as shown in Table 6. The behavior explanation of the measured optical parameters can be found elsewhere [19-23]

Table 6: the transmittance, absorption coefficient, optical properties and optical energy gap of CeO_2: In_2O_3 thin films that have been prepared through using the PLD approach.

Samples	T%	α (cm^{-1})	k	n	ε_r	ε_i	Eg direct(eV)	Eg indirect (eV)
Pure CeO2	86.70	7139	0.031	1.727	2.981	0.108	3.00	-
CeO23%In2O3	65.43	21216	0.093	2.344	5.484	0.435	2.90	-
CeO2:5%In2O3	68.67	18798	0.082	2.265	5.122	0.373	2.85	-
CeO2:7%In2O3	69.34	18309	0.080	2.248	5.045	0.360	2.90	-
CeO2:9%In2O3	61.70	24153	0.106	2.426	5.876	0.513	1.55	1.4

Conclusions

Erbium and indium oxides doped cerium oxide thin films were polycrystalline with cubic fluorite phase. Continuous addition of Eu_2O_3 and In_2O_3 to CeO_2 led to a non-regular increase in the crystallite size. The increase of Eu_2O_3 doping led to a pronounced growth of crystallite size while doping with In_2O_3 led to a less noticeable growth of crystallite size. Dramatic reduction of the energy band gap from 3.0 to 1.2 eV accompanied the addition of 7%Eu_2O_3 to the starting material; also, a red shift occurs that led to reduced energy from 3 to 1.55 eV by continuous addition of In_2O_3 the ceria matrix. This qualifies Eu_2O_3 and In_2O_3 doped ceria for solar cell applications.

References

[1] Y. Castro, B. Julian, B. Viana, H, Amenitsch, C. Boissiere, B. Viana, D. Grosso, C. Sanchez," Synthesis, characterization and optical properties of Eu_2O_3 mesoporous thin films," *Nanotechnology*, vol. 18, no. 5, pp. 055705, 2007

[2] J. Kugai, S. Velu, and C. Song, "Low-temperature reforming of ethanol over CeO_2-supported Ni-Rh bimetallic catalysts for hydrogen production," *Catalysis Lett.*, vol. 101, pp. 255-264, 2005

[3] F.C. Chiu, and C.-M. Lai, "Optical and electrical characterizations of cerium oxide thin films," *J. Phys. D: Appl. Phys.*, vol. 43, no. 7, p. 075104, 2010.

[4] L. Tye, N.A. El-Masry, T. Chikyow, P. McLarty, S.M. Bedair, "Electrical characteristics of epitaxial CeO_2 on Si(111)," *Applied Physics Letters*, vol. 65, p. 3081, 1994.

[5] Z. Yu, Q. Wang, Y. Ma, L. Wang, "X-ray diffraction and spectroscopy study of nano-Eu_2O_3 structural transformation under high pressure," *Journal of Alloys and Compounds*, vol. 701, pp. 542-548, 2017.

[6] A. Kadhim, F. T. Noori, N. D. Hamza, " Optical and Structural Properties of (In_2O_3:ZnO:Au) Nanocomposite Thin Films Prepared by Spray Pyrolysis Method, " *Engineering and Technology Journa*l, Vol. 36, part B, no. 1, pp. 53-58, 2018.

[7] A. Goswami, "Thin Film Fundamental". New Age International (P) Limited publishers, New Delhi, 1996.

[8] Z. Wang, Z. Quan, J. Lin, "Remarkable changes in the optical properties of CeO_2 nanocrystals induced by lanthanide ions doping," *Inorg. Chem.*, vol. 46, no.13, pp. 5237-5242, 2007.

[9] S. K. Sharma, P. Thakur, Shalendra Kumar, D. K. Shukla, N. B. Brookes, C. G. Lee, K. R. Pirota, B.H. Koo, and M. Knobel," Room temperature ferromagnetism in Fe-doped CeO_2 thin films grown on $LaAlO_3$ (001)," *Thin Solid Films*, vol. 519, no. 1, pp. 410-413, 2010.

[10] Z. Fandi, N. Ameur, F.T. Brahimi, S. Bedrane, R. Bachir, "Photocatalytic and corrosion inhibitor performances of CeO_2 nanoparticles decorated by noble metals:Au, Ag, Pt," *J. Environ. Chem. Eng*. vol. 8, no. 5, p. 104346, 2020.

[11] M. M. Khan, S.A. Ansari, M.O. Ansari, B.K. Min, J. Lee, M.H. Cho, "Biogenic fabrication of Au@CeO_2 nanocomposite with enhanced visible light activity," *J. Phys. Chem. C*, vol. 118, no. 18, pp. 9477–9484, 2014.

[12] H. H. Abbas, B. A. Hasan," The Effect of Silver Oxide on the Structure and Optical Properties of ZnO:AgO Thin Films," *Iraqi Journal of Science*, vol. 63, no. 4, pp. 1526-1539, 2022.

[13] M. M. Khan, S. A. Ansari, D. Pradhan, D. H. Han, J. Lee, M. H. Cho, "Defect-Induced band gap narrowed CeO_2 nanostructures for visible light activities," *Ind. Eng. Chem. Res.*, vol. 53, no. 23, pp. 9754– 9763, 2014.

[14] Q. Zhou, S. Ma, S. Zhan, "Superior photocatalytic disinfection effect of Ag-3D ordered mesoporous CeO_2 under visible light," *Appl. Catal. B: Environmental*, vol. 224, pp. 27–37, 2018.

[15] J. Zhang, J. Guo, W. Liu, S. Wang, A. Xie, X. Liu, J. Wang, Y. Yang," Facile preparation of M^{n+}doped (M=Cu, Co, Ni, Mn) hierarchically mesoporous CeO_2 nanoparticles with enhanced catalytic activity for CO oxidation," *Eur J Inorg Chem.*, vol. 2015, no. 6, pp. 969-976, 2015.

[16] H. Li, G. Lu, Y.Wang, Y. Guo, Y. Gue" Synthesis of flower-like La or Pr-doped mesoporous ceriamicrospheres and their catalytic activities for methane combustion," *Catal. Commun.*, vol. 11, no. 11, pp. 946-950, 2010.

[17] A. Bouhlala, W. T. Halais, M. Doghmane, S. Chettibi, " Silver impurities effects on CeO_2 structural, electronic, magnetic, and optical properties: ab initio study, " *Eur.Phys J.B*, vol. 95, article no. 174, 2022.

[18] T. VindoKumar, D. Naga Durgasti, Beniaram M. Reddy, Ivo Alxneit, " Synthesis and Structural Characterization of Eu_2O_3 Doped CeO_2: Influence of Oxygen Defects on CO Oxidation," *Catal Lett.*, vol. 144, pp. 2033-2042, 2014.

[19] B. A. Hasan, "Investigation the Structural and Optical Properties of AgSbSe2 Photoconductor," *Australian Journal of Basic and Applied Sciences*, vol. 9, no. 23, pp. 97-104, 2015.

[20] B. A. Hasan, "role of sulfur content on the photo detection parameters of AgSb (SxSe1-x)2 thin films," I.J.S.N., vol. 8, no. 4, 2017.

[21] B. A. Hasan,,S. S. Mahmood, H. H.Issa, T. T. Issa, "Structural, Morphology and Optical Properties of AlxSb1-x Thin Films Prepared by Pulsed Laser Deposition (PLD)," AIP Conference Proceedings, vol. 2372, p. 040010, 2021.

[22] B. A. Hasan, "Effect of Thickness on the Performance of Bi_2S_3 Thin Film for Photovoltaic Devices," *International journal of advanced scientific and technical research*, vol. 3, no. 4, pp. 103-120, 2014.

[23] B. A. Hasan, M. Abdalhur Kadhim, "Structure, Morphology and Optical Properties of ThermallyEvaporated Cu_2S Thin Films Annealed at Different Temperatures", AIP Conference Proceedings, vol. 2144, no. 1, p. 030021, 2019.